Rapid #: -22611839

CROSS REF ID: **353075864700001852**

LENDER: **GPM (Georgia Southern University) :: Main Library**

BORROWER: **ORU (University of Oregon) :: Main Library**

TYPE:	Article CC:CCL
JOURNAL TITLE:	Engineering geology
USER JOURNAL TITLE:	Engineering geology
ARTICLE TITLE:	Estimating the rainfall threshold of a deep-seated landslide by integrating models for predicting the groundwater level and stability analysis of the slope
ARTICLE AUTHOR:	Wei, Zhen-lei ; Lü, Qing ; Sun, Hong-yue ; Shang,
VOLUME:	253
ISSUE:	
MONTH:	
YEAR:	2019
PAGES:	14 - 26
ISSN:	0013-7952
OCLC #:	38907779

Processed by RapidX: 5/22/2024 6:00:30 AM

This material may be protected by copyright law (Title 17 U.S. Code)

Engineering Geology 253 (2019) 14–26

Contents lists available at ScienceDirect

Engineering Geology

journal homepage: www.elsevier.com/locate/enggeo

Technical note

Estimating the rainfall threshold of a deep-seated landslide by integrating models for predicting the groundwater level and stability analysis of the slope

Zhen-lei Wei[a], Qing Lü[a], Hong-yue Sun[b,*], Yue-quan Shang[a]

[a] College of Civil Engineering and Architecture, Zhejiang University, Hangzhou 310058, China
[b] Ocean College, Zhejiang University, Hangzhou 310058, China

ARTICLE INFO

Keywords:
Deep-seated landslides
Rainfall threshold
Groundwater

ABSTRACT

Rainfall thresholds of landslides often are determined by empirical meteorological thresholds, but the reliability of this approach sometimes is limited by the lack of information about the hydrological processes that trigger landslides. Groundwater plays a critical role in triggering deep-seated landslides. In this study, we propose a methodology to estimate the rainfall threshold for a deep-seated landslide based on an integrated model that combines a model for predicting the level of the groundwater with a finite-element, strength-reduction model. First, in order to obtain more accurate results when predicting the level of the groundwater, a method is proposed to estimate the groundwater level fluctuation caused by rainfall (GLFR). Then, two different machine learning methods, i.e., the genetic algorithm back-propagation neural network (GA-BPNN) method and the genetic algorithm support vector machine (GA-SVM) method, are proposed for predicting the GLFR of the Duxiantou landslide located in Zhejiang Province, China. The results of the predictions showed that the performance of the GA-SVM model was better than that of the GA-BPNN model. Then, a series of numerical simulations was conducted to investigate the factor of safety (Fs) of the slope at different groundwater levels. At last, the probabilities of the occurrences of Duxiantou landslides for different return periods of rainfall intensity were evaluated to determine the rainfall threshold.

1. Introduction

Landslides often cause extensive casualties and property losses. The reasons landslides occur are influenced by several known triggering factors, the most frequent of which is rainfall (Mansour et al., 2011). Rainfall often causes multiple processes that decrease the stability of a slope, such as an increase in the positive pore pressure (Matsuura et al., 2008; Simoni et al., 2004; Zhang et al., 2015; Okada et al., 2004; Lin et al., 2018; Sun et al., 2012) and a decrease of suction (Godt et al., 2009). Rainfall thresholds can be divided into two groups, i.e., (1) a physical group that is based on numerical models (Iverson, 2000) and (2) an empirical (statistical) group based on the analysis of historical landslide events and the accompanying rainfall (Guzzetti et al., 2008; Martinović et al., 2018; Marjanović et al., 2011; Chang et al., 2011; Lin et al., 2009; Lee et al., 2013). The empirical rainfall threshold usually is a line that divides the rainfall data into two categories, i.e., (i) rainfall that induced landslides and (ii) rainfall that did not induce landslides. Currently, the empirically-derived thresholds commonly are used (Guzzetti et al., 2008; Peruccacci et al., 2017). However, Berti et al. (2012) indicated that it was difficult to identify a threshold for landslides because rainfall events may or may not result in landslides, which makes it difficult to determine a specific rainfall threshold (Hong et al., 2017). For triggering deep-seated landslides, the role of hydrology has been acknowledged to be of key importance, but it usually is not included in the statistical precipitation I-D threshold approach (Bogaard and Greco, 2018).

For the case of a deep-seated landslide, when the groundwater level is well below the surface of the ground, an increase in the level of the groundwater often induces the landslide. Caris and Asch (1991) conducted geophysical, geotechnical, and hydrological surveys on a specific landslide of black marl material in the French Alps to assess its stability. The results of the analysis indicated that the groundwater level 4 m below the surface was the critical threshold for activating the specific landslide. Mantovani et al. (2000) monitored the Tessina landslide located in northeastern Italy, and they concluded that landslides may be correlated with a sudden increase in the groundwater

* Corresponding author.
E-mail address: shy@zju.edu.cn (H.-y. Sun).

https://doi.org/10.1016/j.enggeo.2019.02.026
Received 22 October 2018; Received in revised form 24 February 2019; Accepted 25 February 2019
Available online 04 March 2019
0013-7952/ © 2019 Elsevier B.V. All rights reserved.

level during the observation period. Zhi et al. (2016) investigated and monitored a rainfall-induced, deep-seated landslide, and they concluded that the groundwater level had a direct connection with the movement of the slope. Therefore, it is very important to evaluate the fluctuation of the groundwater level accurately based on previous rainfall in order to predict the occurrence of a deep-seated landslide. However, the relationship between rainfall and the groundwater level usually is very complicated. The effect of rainfall on the groundwater may depend on the intensity of the rainfall (Jan et al., 2007), evapotranspiration (Baird and Iii, 2005), the morphology of the slope (Schilling, 2009), the thickness of the unsaturated zone, the type of soil, its hydraulic properties, and the existence of preferred paths (Crosta and Prisco, 1999).

To date, two different approaches have been used to explore the fluctuation of the level of the groundwater. One approach uses a physical model, and the other approach uses a phenomenological model (Cascini et al., 2006, 2010). The physical approach attempts to predict the fluctuation of the level of the groundwater by considering the mechanical properties and/or the hydraulic properties of the soil/rock. Hong and Wan (2011) presented a model based on the continuity equation to predict fluctuations of the groundwater level on a hillslope in response to hourly precipitation rates. However, it is very difficult to get some of the required physical parameters for complex landslides, such as hydraulic conductivity, specific yield, and specific storage. Thus, there are some limitations associated with the use of the physical models. The phenomenological model is an empirical approach that is based on the analyses of a series of data gathered by the continuous monitoring of the groundwater levels and rainfall in landslide areas. For the phenomenological approach, the mechanical parameters of the soil/rock and the boundary conditions within the slope can be neglected (Hong et al., 2005; Federico et al., 2012; Zhang et al., 2017), which makes this approach suitable for large and complex landslides in which monitoring data are available but the physical parameters are difficult to obtain. The machine learning methods, which are artificial intelligence methods, have been used extensively to explore the relationship between the groundwater level and the amount of precipitation. Yoon et al. (2011) developed a model using artificial neural networks and support vector machine techniques based on data for the groundwater level, precipitation, and the tide level. Krkač et al. (2017) predicted the fluctuation of the groundwater level via random forests methods for the Kostanjek landslide. Huang et al. (2017) used a particle swarm optimization support vector machine (PSO-SVM) model based on chaos theory to predict the daily groundwater levels of the Huayuan landslide in the Three Gorges Reservoir Area of China. The major advantage of machine learning methods is that they can be used effectively to model flexible, nonlinear behavior. Also, when machine learning methods are used, there is no need to specify a pre-determined model to reflect the relationships between the inputs and the outputs; the models are created adaptively based on the features of the monitoring data. This data-driven approach is suitable for many empirical datasets when no theoretical guidance is available to perform more appropriate data correlation processes (Hong, 2017).

When using machine learning methods to construct a model for predicting the groundwater level, the determination of the output layer is important because it may influence the accuracy of the forecasts. Currently, two different output layers are used, i.e., 1) the elevation of the groundwater level (GL) and 2) the groundwater level fluctuation (GLF), which is defined as the difference between the current and the subsequent GL data. Hong (2017) evaluated the effects of the two different output layers on the accuracy of the forecasts, and he found that the forecasting method that used GLF had much better agreement with the measured values than the use of GL. Also, Krkač et al. (2017) concluded that the predictions of changes in the GLF yielded significantly better results than the direct predictions of GL. To date, most researchers have assumed that GLF is determined only by rainfall. The water inflow from confining aquifers (e.g., upslope or adjacent to the landslide mass) also will have an effect on GLF, but the main source of water flow is the rainfall. So their models that predict GLF are based only on past rainfall data. However, this approach does not seem reasonable because the value of GLF actually is determined by two different factors, i.e., rainfall and natural drainage, and natural drainage is affected mainly by the groundwater level and the hydrogeological conditions of the slope. Thus, in this study, we defined the causes of the fluctuation of the groundwater level as 1) rainfall (GLFR) and 2) drainage (GLFD), where the latter refers to the speed at which the groundwater level decreases.

In this study, we used a hydro-meteorological model to estimate the rainfall threshold of a deep-seated landslide. First, in order to get more accurate predictions of the groundwater level, we proposed a method to calculate the fluctuation of the groundwater level caused by rainfall (GLFR). Then, based on the data obtained from the continuous monitoring of the groundwater level and precipitation, two different machine-learning methods were used to predict the GLFR of the Duxiantou landslide, which occurred in Zhejiang Province, China. The two machine learning methods that we used were the genetic algorithm back-propagation neural network (GA-BPNN) method and the genetic algorithm support vector machine (GA-SVM) method. Then, based on the data obtained by monitoring the groundwater level and the predictions of the groundwater level, a series of numerical simulations was conducted to investigate the factor of safety (Fs) of the slope for different groundwater levels. Therefore, we were able to determine the relationship between the amount of rainfall and the stability of the slope. Also, we investigated the probability of the occurrence of the Duxiantou landslide with different return periods.

2. Study area and the collection of data

The Duxiantou landslide was located near the Longli highway in Zhejiang Province, China. The location is near Duxiantou Village about 10 km from Longyou County (Fig. 1). According to the geological survey, the landslide was a remobilized ancient landslide deposit (Sun and Lü, 2012). On the topographic map of the landslide (Fig. 2), the slope is relatively gentle, i.e., about 20° in the upper part, but, in the lower part, it is relatively steep (about 35°). The soil mass was stable before the excavation work that was done to build the Longli highway. When the construction of the highway was completed, some preventive measures were implemented to ensure the stability of the slope, such as reducing the slope of the trailing edge and increasing the elevation of the highway. However, after continuous heavy rainfall in 2005, the retaining wall at the toe of the slope showed signs of deformation, which included cracks in the retaining walls at the toe, and the surface of the road also underwent upheaval. Thus, some gauges were installed to monitor the groundwater level, and a GPS monitoring system was installed to monitor the surface displacement so the stability of the landslide could be assessed.

Based on the geological investigation report, six exploration boreholes were drilled to have a detailed cross section of the landslide (Fig. 3). The landslide was composed mainly of disintegrated rock mass and unconsolidated Quaternary deposits (Q^4). The unconsolidated Quaternary deposits are composed mainly of gravel soil, which is a mixture of clay and gravel. The most common grain sizes of gravel are in the range of 4–10 cm. The hydraulic conductivity of the gravel soil is about 0.00018 m/s. The value of the hydraulic conductivity was selected based on the geological investigation report, and it was determined by a well-pumping test in the field. The underlying bedrock was crystal tuff of upper Jurassic. This landslide was deemed to have slipped along the interface (a planar surface) between the Quaternary deposits and the upper Jurassic bedrock. The average thickness of the sliding zone was about 1 m (Sun and Lü, 2012). The front edge of the landslide was about 500 m wide along the road extension, and the horizontal length of the landslide was about 210 m, as shown in the vertical cross-section (Fig. 3). The average thickness of the body of the

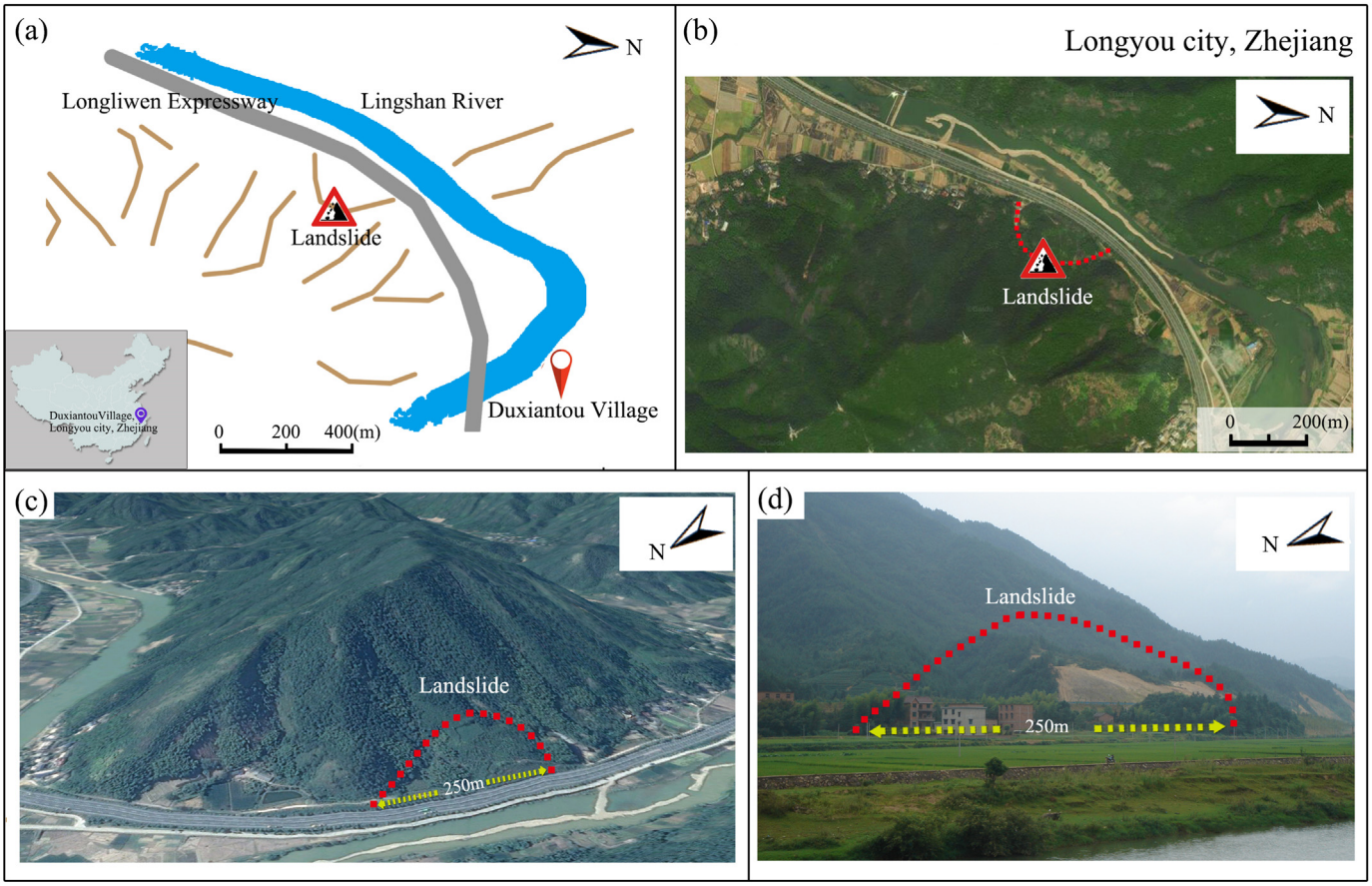

Fig. 1. Location and appearance of the Duxiantou landslide.

landslide was about 23 m, so the total volume of the landslide was about 1.600.000 m^3.

Five hydrological boreholes were drilled in 2006 to monitor the groundwater level. However, during the monitoring period, three of the five boreholes (ZK2, ZK4, and ZK5) were destroyed when they collapsed due to the poor quality of the construction. Thus, only two boreholes (i.e., ZK1 and ZK3 in Fig. 4) have been working continuously. An automatic water-level recorder was installed at the bottom of each borehole. The depths of the two boreholes are 24 m (ZK1) and 25 m (ZK3), respectively. The recorders sample the water level every 30 min with a resolution of 0.8 mm, and they are used to measure the level of the groundwater in the hydrological holes. Also, a rain gauge was installed on the roof of a house that is located about 200 m from the landslide. The rain gauge was an HOBO RGM-3 automatic rainfall tipping-bucket recorder, and it was obtained from the Onset Company (USA). The rain gauge samples the rainfall with a minimum value of 0.2 mm.

3. Analysis of the correlation between the groundwater level and rainfall

Fig. 4 shows the observations of the GL response to rainfall for two consecutive years. Unfortunately, monitoring data was missing during the January and February in 2009 because the battery of the monitoring recorder was dead. Fig. 4a shows the observations of the GL

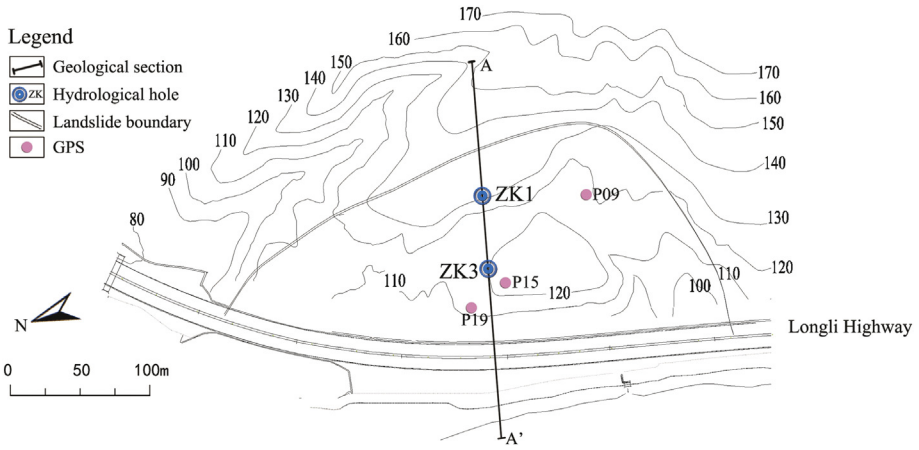

Fig. 2. Topographical map of the Duxiantou landslide and location of the monitoring network.

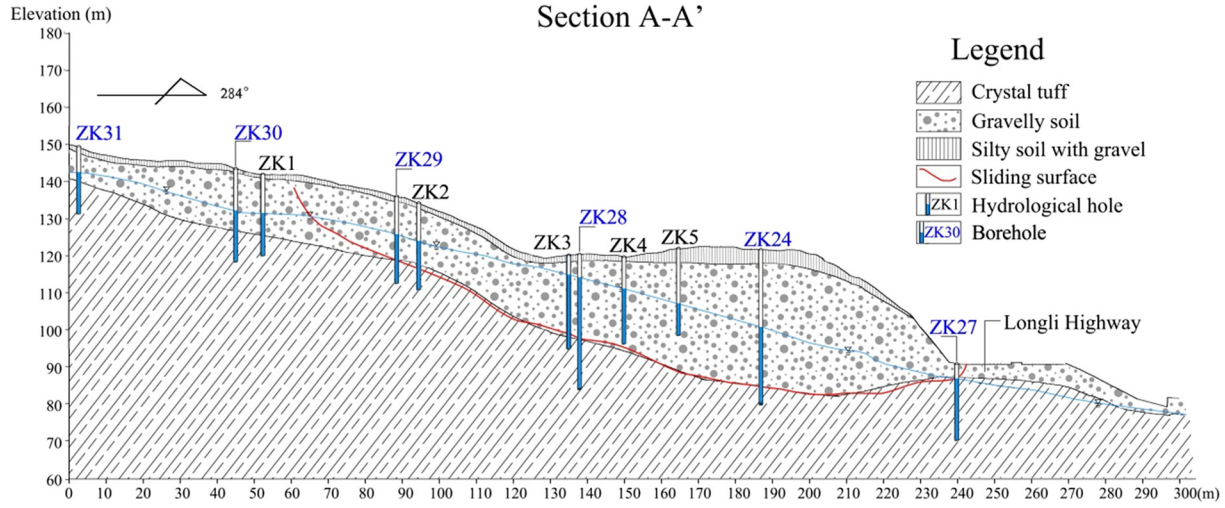

Fig. 3. Geological cross-section (A–A′) of the Duxiantou landslide.

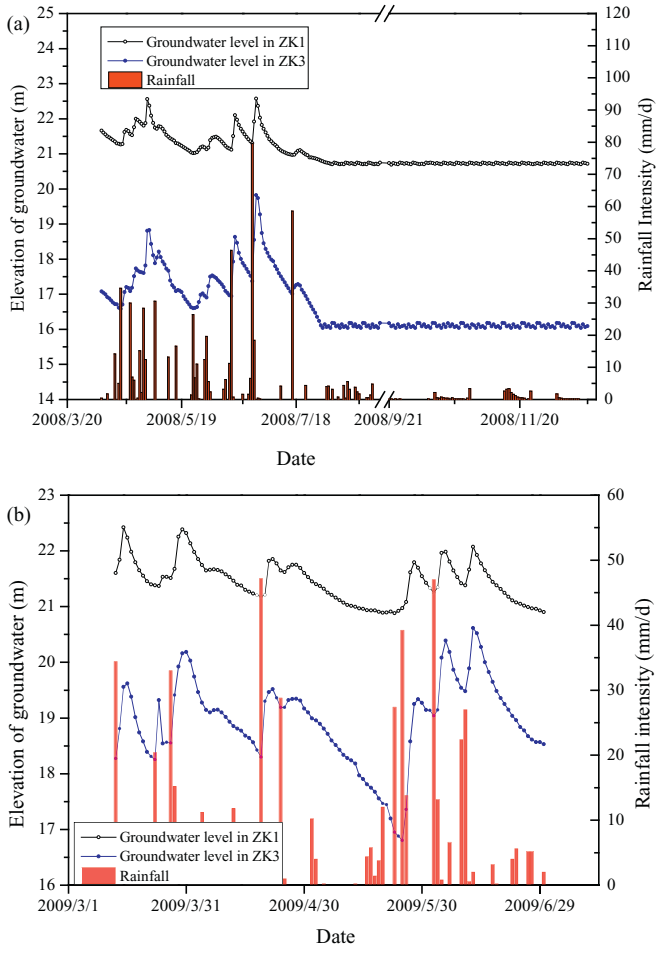

Fig. 4. Relationship between rainfall and GL: (a) monitoring recording in 2008; (b) monitoring recording in 2009.

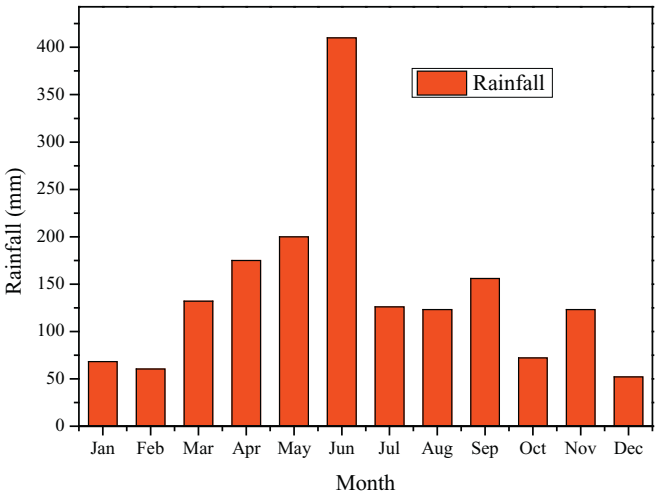

Fig. 5. Distribution of monthly-average rainfall.

response to rainfall from April through December in 2008. It was observed that the hydrological response of the landslide varied greatly in different seasons. The groundwater level usually was high from April through June because the largest amount of precipitation occurred during this period. Fig. 5 shows the distribution of the monthly-average rainfall for a nine-year period (2009–2018) at Lonyou station, which is located about 10 km from the site of the landslide. Fig. 5 shows that most of the rainfall each year occurred from April through June, and there was much more rainfall in June than in the other months. This indicates that the hydrological recording of the period from April through June was very important because of the extensive rainfall during this period. In addition, the relative variations of the groundwater level also were drastic from April through June, which provided a good opportunity to explore the relationship between rainfall and the groundwater level. After June, the groundwater level decreased and it reached a low level from September through December because there was very little precipitation. The variations of the groundwater level from September through December also were negligible. Since high groundwater levels have been confirmed to have a critical role in triggering deep-seated landslides, the period from April through June can be considered the most critical period for the stability of the slope. In this study, it was found that the monitoring recording of two consecutive hydrological years, i.e., 2008 and 2009, included the period from April through June. Thus, we concluded that the data that were recorded during this period provided the most critical hydrological response at the site of the landslide. It has been demonstrated that the rainfall thresholds of shallow landslides are affected strongly by seasonal effects (Pirone et al., 2015a, Pirone et al., 2015b; Urciuoli et al., 2016; Cascini et al., 2014). The matric suction and volumetric water content change from season to season, so the season strongly affects the spatial distribution and the type of slope instability that is likely to

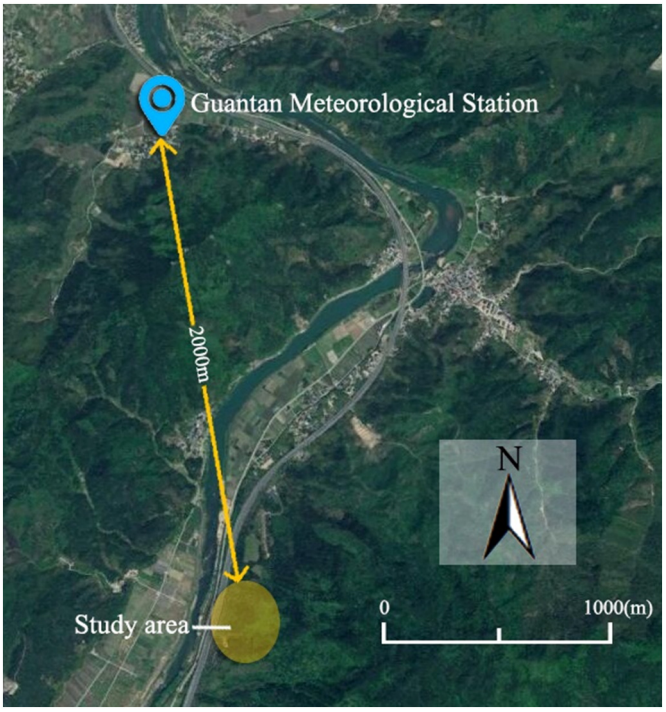

Fig. 6. Location of the Guantan meteorological station and the study area.

develop. However, most deep-seated landslides of 5–20 m in depth are sensitive to rainfall and are prone to sliding due to the increase in the pressure of the pore water on the slip surface induced by the rising groundwater level (Van Asch et al., 1999). For shallow landslides or debris flows, failure conditions can occur when, at a critical depth (< 5 m), which is determined mainly by the cohesion of the soil mass and the angle of the slope, the moisture content in the soil approaches saturation, which reduces the matric suction in the unsaturated soils, resulting in a considerable reduction in the strength of the soil (Van Asch et al., 1999). The mechanisms that induce shallow landslides and deep-seated landslides are different. Changes in the matric suction and in the volumetric water content in the surface soil (0–5 m) are not as important as the increasing groundwater level for triggering deep-seated landslides.

In addition, in order to further verify that the characteristics of monitoring rainfall events and the actual rainfall characteristics of landslide sites are similar, we also conducted a magnitude-frequency analysis. We collected the rainfall records from the Guantan meteorological station, which was established in 2014. The Guantan station is located about 2 km from the landslide site (Fig. 6). Both the station and the landslide site are located on the bank of the river. The station and the rain gauge are at approximately the same elevations. The topographic conditions of the landslide site and Guantan station are similar, so the spatial variability of the rainfall is small. Fig. 7 shows the rainfall that was recorded at Guantan station from 2014 to 2018. The durations of the monitoring recordings at the landslide site were April through December in 2008 and March through July in 2009. We conducted a magnitude-frequency analysis of the rainfall, and Fig. 8 shows the comparison results of the cumulative frequency distribution. Fig. 8 also shows that the magnitude frequency curves of the three monitoring periods were similar. This means that the monitoring recordings reflected the actual rainfall characteristics at the landslide site.

Fig. 4 indicates the relationship between GL and rainfall in both boreholes. The GL response generally consisted of a rapid increase followed by a slower decrease, and the peak GL often occurred after the rainfall had stopped. The depth of the groundwater was evaluated from the bottom of each borehole. Fig. 4 shows that there was a time lag

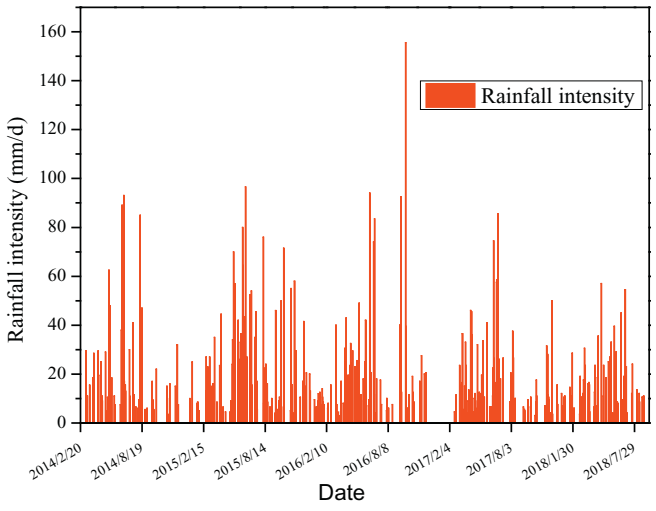

Fig. 7. Distribution of rainfall for 2014–2018 at Guantan station.

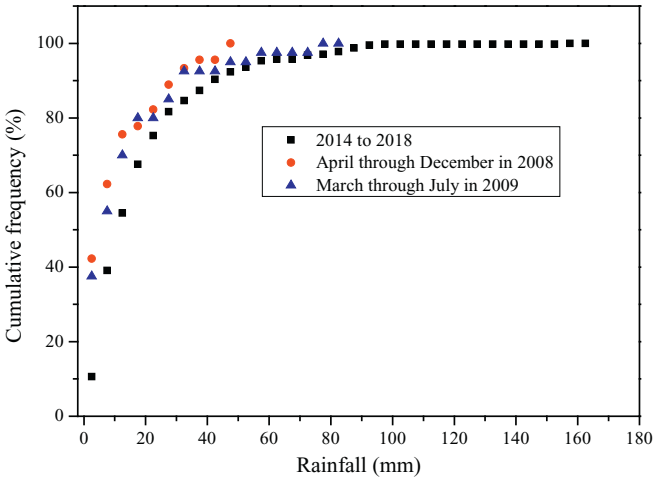

Fig. 8. Comparison of the monitoring recording of cumulative frequency distribution and the recording of cumulative frequency distribution from Guantan Station.

between the time when the maximum precipitation occurred and the time of when the groundwater level was at its highest level. This phenomenon is well understood because it takes some time for the infiltration of the rainfall to occur and affect the groundwater level. The lag time depended mainly on the hydraulic conductivity of the soil.

Fig. 9 shows that the response of GLF and rainfall had similar fluctuation trends in both of the groundwater monitoring boreholes. However, the olive dashed lines in Fig. 9 show that, even though some rainfall events occurred, the corresponding value of GLF was still negative, so this approach does not seem reasonable. This phenomenon also was observed Krkač et al. (2017) and by Huang et al. (2017). Actually, GLF consists of two parts, i.e., one part is caused by rainfall (GLFR), and the other part is influenced by natural drainage, which determines the speed at which the groundwater level (GLFD) decreases. Eq. (1) shows the relationships of GLF, GLFR, and GLFD.

$$GLF = GLFR + GLFD \quad (1)$$

The GLFD usually is affected by the groundwater level and by the hydrogeological conditions of the slope. High groundwater levels usually are associated with large GLFD in order to maintain the groundwater balance in the body of the slope; in addition, the high GL also means that a high hydrological gradient exists within the slope, which means there will be a high outflow of water. According to Eq. (1),

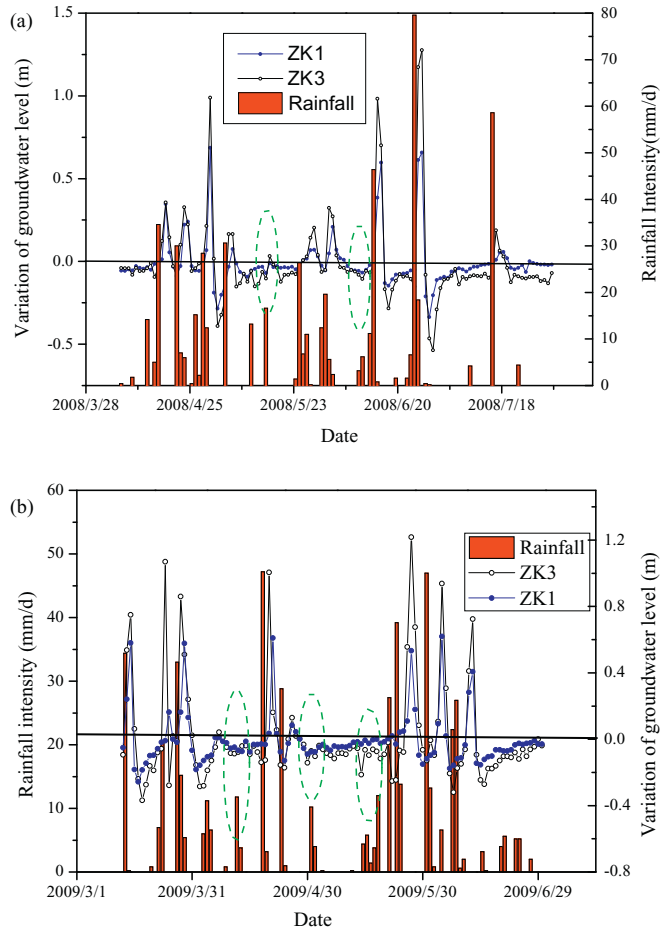

Fig. 9. Relationship between rainfall and GLF: (a) monitoring recording in 2008; (b) monitoring recording in 2009.

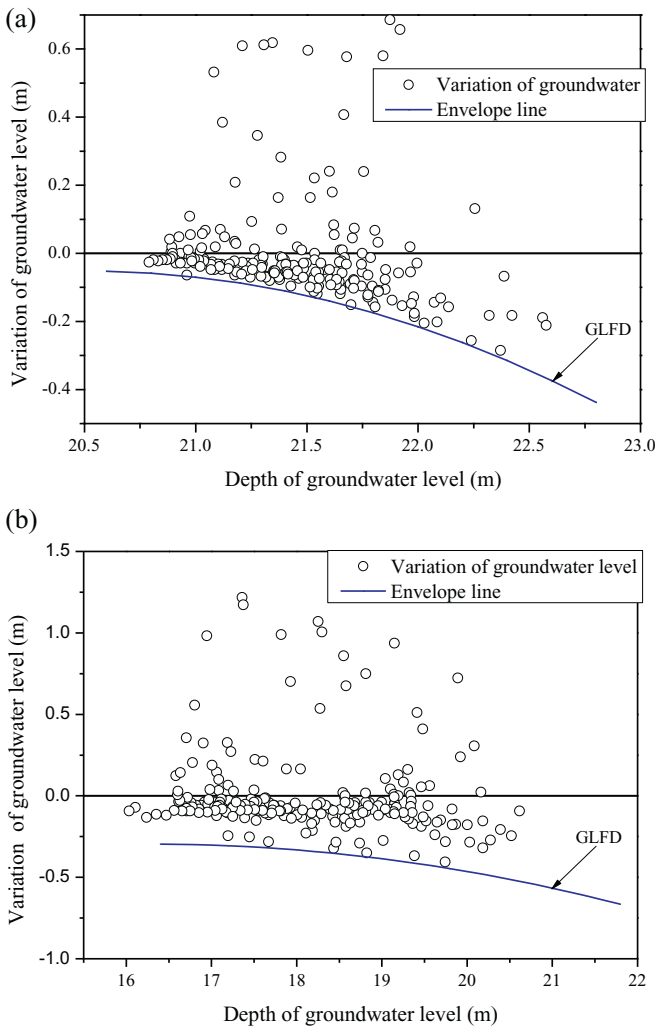

Fig. 10. Values of GLF and the corresponding GL values: (a) ZK1; (b) ZK3.

when the value of GLFR is zero, which means there was no precipitation, the GLF is equal to the GLFD. So, it was considered that the lower enveloping curve (f(x)) represented the values of GLFD for different values of GL when there was no precipitation. To determine the value of GLFD, we present the values of GLF and the corresponding GL, as shown in Fig. 10. We considered the lower enveloping curve (f(x)) to be the values of GLFD for different values of GL when there was no precipitation.

The lower enveloping curves, (f(x)), in ZK1 and ZK3 are expressed as Eqs. (2) and (3), respectively. The lower enveloping curves were calculated based on 240 data points. Eqs. (2) and (3) were determined by automatic fitting. Eqs. (2) and (3) also have the minimum standard error.

$$y_{zk1} = -30.9715 + 3.015 \times x_1 - 0.0735 \times x_1^2 \quad (2)$$

$$y_{zk3} = -3.4886 + 0.392 \times x_2 - 0.01207 \times x_2^2 \quad (3)$$

where y_{zk1} and y_{zk3} are the values of GLFD in ZK1 and ZK3, respectively, for different GL values, and x_1 and x_2 are the corresponding groundwater levels in ZK1 and ZK3, respectively. Note that the proposed method has some limitations, one of which is that the method is an empirically-based method, and Eqs. (2) and (3) are only suited for the study of the landslide. Another limitation is that the envelope will be affected by the history of actual rainfall events.

The values of GLFD in ZK1 and ZK3 can be obtained from Eqs. (2) and (3). Then, the values of GLFR can be obtained by substituting GLFD and GLF in Eq. (1), and they are shown in Fig. 11.

Fig. 11 shows that the GLFR and rainfall now have similar fluctuation trends in both boreholes. When we exclude the effect of GLFD, the GLFR is determined only by the rainfall. So, the value of GLFR is always positive when precipitation occurs.

4. An integrated model to estimate the rainfall threshold of a deep-seated landslide

In this section, based on the calculation of GLFR, we developed a rainfall threshold model in which we combined the forecasting model of GLFR with two numerical processes. First, two non-linear models, i.e., the Genetic Algorithm Support Vector Machine (GA-SVM) and the Genetic Algorithm Back-Propagation Neural Network (GA-BPNN) models, were considered for forecasting variations in the GLFR based on the antecedent rainfall. Then, a numerical procedures, i.e., the finite element shear strength reduction method (FE-SSR) was used to compute the factor of safety (Fs) of the Duxiantou landslide based on monitoring and predicting the groundwater level.

4.1. Prediction of GLFR based on antecedent rainfall

4.1.1. GA-BPNN model

Back-propagation (BP) neural networks are among the most extensively used neural network algorithms (Lü et al., 2012). They are well known for their good self-learning, self-adapting, robustness, and generalization ability. However, the BP algorithms also have some disadvantages, such as a poor rate of convergence and easily getting stuck in the local minimum. The genetic algorithm (GA), one of the

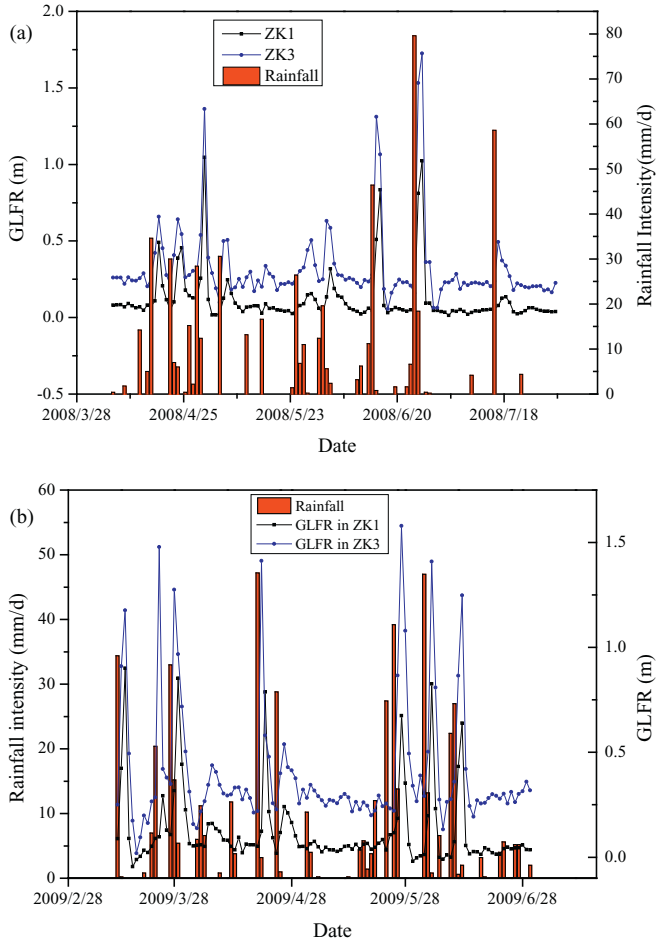

Fig. 11. Relationship between GLFR and rainfall: (a) monitoring recording in 2008; (b) monitoring recording in 2009.

evolutionary algorithms, is a heuristic, stochastic, search algorithm. The GA has good global searching ability and can learn the near-optimum solution without the gradient information of error functions, so it is a powerful tool for optimization, searching, and machine learning. In this context, the connection weights of the neural networks were optimized using GA in order to overcome the disadvantage of easily getting stuck in the local minimum.

4.1.2. GA-SVM model

The SVM is another kind of non-linear regression forecasting method that was proposed by Cortes and Vapnik (1995). The input variables are mapped into a higher-dimensional feature space through a non-linear transformation, a process that is used extensively in geotechnical engineering (Ji et al., 2016). In order to build an effective SVM model, the parameters of the model (C_s and γ) must be chosen properly in advance (Li and Kong, 2014). The C_s is named as penalty parameter and the γ is named as kernel parameter. The parameter, C_s, determines the tradeoff cost between minimizing the training error and the complexity of the SVM model. With a larger C_s value, the predictive accuracy of the training sample is better. However, this may cause an over-training problem. The parameter, γ, of the RBF kernel function defines a nonlinear mapping from the input space to the high-dimensional feature space. Hence, the parameters C_s and γ influence the efficiency and generalization performance of the SVM model (Zhou et al., 2016). GA is an adaptive optimizing method with overall searching function. In order to avoid the blindness of the parameter selection of the SVM model, in this study, we mainly used GA to search for the optimal parameters, i.e., C_s and γ, of the SVM model for prediction. The main advantage of the SVM is that the model is a learning method based on small samples. It is different from traditional statistics theory and neural network methods, which are suitable for big samples. Comparing the methods, the SVM method has a solid theory foundation, easily deals with high-dimensional and nonlinear problems, and can avoid local minimum and dimension disaster problems in BPNN methods. The disadvantage of the SVM mainly lies in its complicated theory, the generalization performance of the SVM models strongly depends on the right choice of its kernel functions and the parameters (C_s and γ) Hence, it is vitally important to reasonably determine them.

In order to verify the accuracy of the models' predictions, we used the Root Mean Square Error (RMSE) and the Relation Index (RI), as defined below:

$$RMSE = \sqrt{\frac{1}{N}\sum_{i=1}^{N}(y_i - x_i)^2} \tag{4}$$

$$RI = \sqrt{1 - \frac{\sum_{i=1}^{N}(y_i - x_i)^2}{\sum_{i=1}^{N}(x_i - \bar{x}_i)^2}} \tag{5}$$

where x_i is the measured value; y_i is the predicted value; x_i is the average value of the sequence; and N is the number of predicted values.

4.1.3. Results of the prediction of GFLR

The predicted value of GLFR at a future time usually is considered to be a function of the precipitation that has occurred in the previous several days and the current precipitation. The influence period of antecedent precipitation depends mainly on the hydrological conductivity of the body of the landslide, and the topic concerning effective antecedent precipitation has been debated extensively in the literature. For different cases, the effective levels of antecedent precipitation were different. In this study, we used the Pearson correlation method to determine the duration of the influence (Dai and Lee, 2001). The Pearson correlation was calculated using SPSS software. The larger the value of the Pearson correlation coefficient becomes, the more relevance there is between the variables. We considered the variables in the correlation analysis to be the GLFR in ZK1 and ZK3, the precipitation on an earlier day (S_1), the sum of the precipitation on two earlier days (S_2), the sum of the precipitation on three earlier days (S_3), the sum of the precipitation on four earlier days (S_4), the sum of the precipitation on five earlier days (S_5), the sum of the precipitation on six earlier days (S_6), and the sum of the precipitation on seven earlier days (S_7). Table 1 shows the Pearson correlation coefficient between GLFR in ZK1, ZK3, and the different precipitation times.

Table 1 shows that S_2 had the best correlation with GLFR in both boreholes. This means that the precipitation that occurred two days earlier had a significant impact on GLFR. In contrast, the S_1 had a relatively small correlation coefficient, indicating that the effect of S_1 on GLFR was minor. Table 1 shows that the calculated Pearson correlation coefficients were 0.76, 0.72, 0.63, 0.54, 0.47, and 0.43 for S_2, S_3, S_4, S_5, S_6, and S_7, respectively. The correlation coefficients will decrease with the passage of time, which means that the effect of precipitation will

Table 1
Pearson correlation coefficient of different precipitation times.

Pearson correlation coefficient	ZK1	ZK3
S_1	0.35	0.54
S_2	0.76	0.78
S_3	0.72	0.74
S_4	0.63	0.66
S_5	0.54	0.58
S_6	0.47	0.48
S_7	0.43	0.44

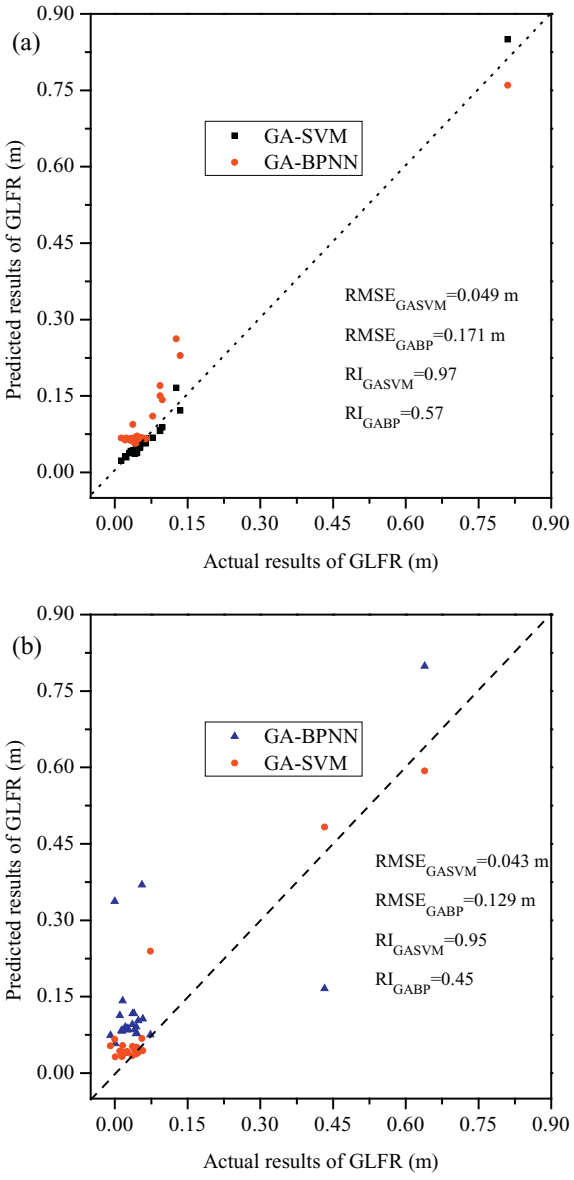

Fig. 12. Comparison of the forecasted results and the actual results in ZK1: (a) comparison results in 2008; (b) comparison results in 2009.

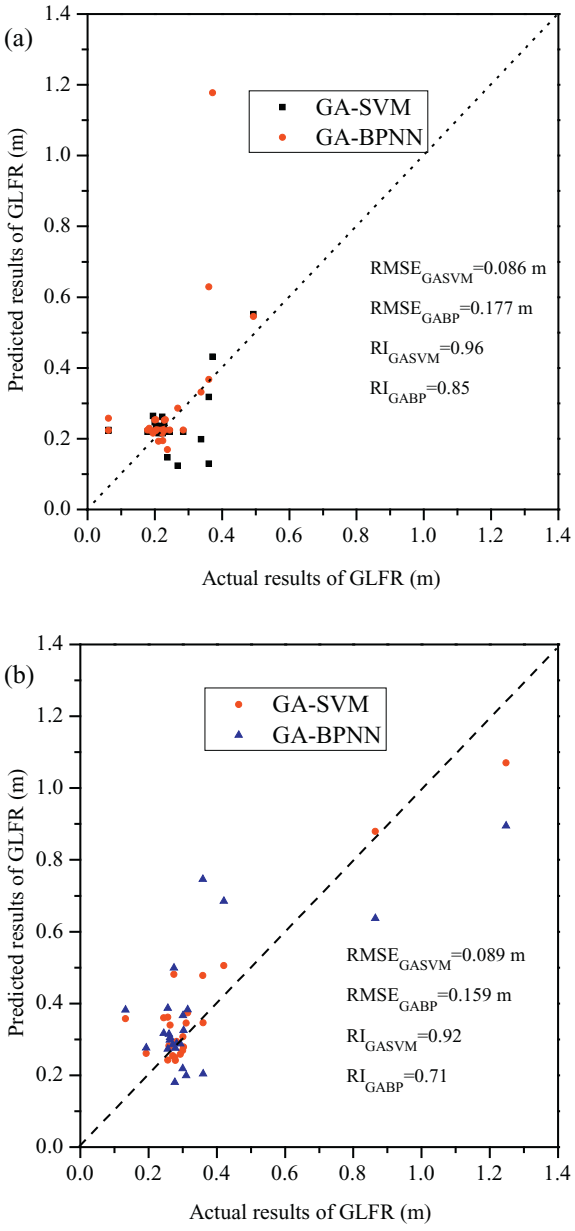

Fig. 13. Comparison of the forecasted results and the actual results in ZK3: (a) comparison results in 2008; (b) comparison results in 2009.

diminish with the passage of time. If the Pearson correlation was > 0.6, it meant that a high correlation existed among the independent variables (Han et al., 2017). The correlation coefficient of S_5 was < 0.6, so, considering the results of the correlation analysis, we used 96 h (four days)as the duration of the influence.

Based on the previous study, the input parameters were defined as precipitation in the same day (P_0), precipitation one day earlier (P_1), precipitation two days earlier (P_2), precipitation three days earlier (P_3), and precipitation four days earlier (P_4); the GLFR of a future time was regarded as the output parameter. Then, we chose the precipitation from March 13, 2009 through June 5, 2009 and the precipitation from April 7, 2008 through June 25, 2008 (78% of the database) as the training samples. We chose the precipitation from June 6, 2009 through June 29, 2009 and the precipitation from June 26, 2008 through July 25, 2008 (22% of the database) as the test samples to verify the reliability of the models. Figs. 12 and 13 show the comparison of the forecasted results and the actual results of the GA-BPNN and GA-SVM models in ZK1 and ZK3.

Figs. 12 and 13 show that the performance of GA-SVM was better than that of GA-BPNN in both boreholes. Therefore, the GA-SVM model can better represent the relationship between the influencing factors and GLFR and produce a better prediction of the GLFR. We concluded that the GA-SVM models performed better than the GA-BPNN model because they were fitted based on the limited number of samples that were available in this study. The GA-BPNN model was more suitable for problems for which a large amount of sampling data was available. Although the GA-BPNN model had good global searching ability and can determine the near-optimum solution without the gradient information of error functions, it performed well only if the network of the problem had an appropriate structure. In addition, it was very sensitive to the number of samples, and the limited samples in the calibration set led to insufficient training of the model, which explains why the predictions of the GA-BPNN model were not ideal. For any algorithm, the quantity and quality of samples have significant impacts on the accuracy of the algorithm's predictions. However, the GA-SVM model is a learning method based on small samples; thus, when building a model to use it, not many training samples are required (Li and Kong, 2014; Zhou et al., 2016). In addition, for computing of

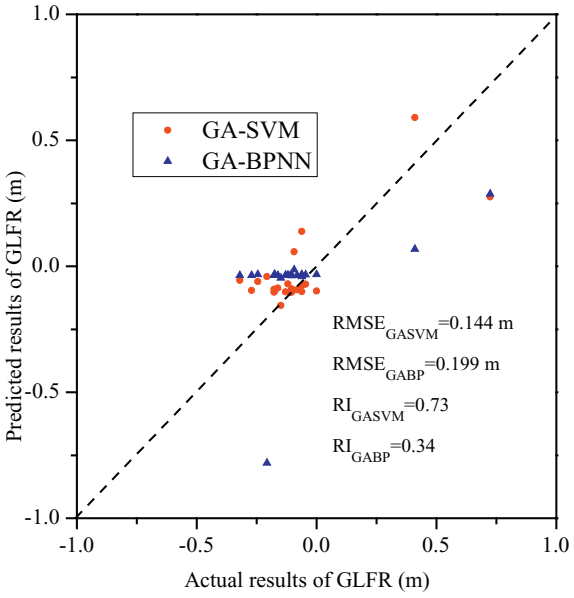

Fig. 14. Comparison of the forecasted results and the actual results using GLF in ZK3.

models, the GA-SVM models only need to optimize two free parameters, whereas GA-BPNN requires many parameters (i.e., hidden nodes, a learning rate, a momentum term, and training epochs), and it is very difficult to obtain these optimal parameters at the same time (Cai et al., 2016).

In addition, in order to evaluate the effect of GLFD on the accuracy of the forecasted results, we just regarded the GLF in 2008 as the output parameter. Fig. 14 shows the verification results for ZK3.

Fig. 14 shows that the RMSE and RI of the GV-SVM model were 0.144 and 0.73, respectively, and that the RMSE and RI of the GABP were 0.199 and 0.341, respectively. Compared with the calculated results of GLFR, there will be a negative effect on calculating GLF. The RMSE increased from 0.089 to 0.144, and the RI decreased from 0.95 to 0.73 for the GA-SVM model. Thus, the effect of GLFD on forecasting the GLF must be considered.

4.2. Evaluation of the stability of the slope based on numerical procedures

As highlighted in Section 4.1, we developed the relationship between rainfall and GLF. In order to determine the critical threshold of the groundwater level that could reactivate the landslide, a series of numerical computations were conducted to investigate the factor of safety (Fs) of the slope for different values of GL. The method was the finite element shear strength reduction (FE-SSR) method, which was computed via the commercial code of Phase 2 (www.rocscience.com). The Section A-A' was selected as the section to be used for the computation. The initial groundwater level also was set based on the geological investigation report. We assumed that the soil below the groundwater table was saturated and that the soil above the water table was dry (unsaturated). The entire numerical model was constrained on the two lateral boundaries in the horizontal direction and at the bottom boundary in both the vertical and horizontal directions. The FE-SSR model projected a length of 290 m and a height of 150 m, as shown in Fig. 15. The model was discretized into 2719 6-node triangular elements. The soil model used an elastic, perfectly-plastic model of a fixed yield surface defined by the Mohr-Coulomb failure criterion. The factor of safety (Fs) of the slope was computed by the shear strength reduction technique (Dawson et al., 1999). Table 2 provides the properties of the soil and rock, which were set based on the engineering geological investigation report. The samples for the tests were taken from the ZK28 and ZK24 boreholes (as shown in Fig. 3). For ZK28, the sample was taken at a depth of 20.55–20.75 m, which was the sliding zone. For ZK24, the sample was taken at a depth of 27.43–27.63 m, which was the gravel soil. The properties of the samples were determined based on direct shear tests in the saturated condition. The properties of the soil also were confirmed through back analysis in the engineering geological investigation report.

Then, we calculated the value of Fs of the Duxiantou landslide for eight representative values of GL in the monitoring period. The elevation of the GL refers to the level from the bottom of the boreholes. In this study, we considered the slope to be in an unsteady state when the value of Fs was < 1. Table 3 provides the Fs values that were obtained.

Table 3 indicates the values of GL that determined the stability of the slope. The value of Fs was 1.423 when there was no groundwater level, implying that the condition of the slope is safe. However, as GL increased, the value of Fs decreased from 1.146 to 1.045. For each 1-m increase in GL, Fs decreased by an average of 0.2. It is apparent that the values of GL have significant effects on the values of Fs, i.e., the larger GL becomes, the smaller Fs becomes. Therefore, if we could predict the value of GL accurately for different precipitation conditions, we could evaluate the stability of the slope. As noted in Section 4.1, we can predict the value of GLF accurately using the GA-SVM model. So, we developed the relationship between the rainfall and the stability of the slope, and we provided an approach that can be used to determine the rainfall threshold that could trigger a rainfall-sensitive landslide.

We used the GPS measurement data to verify the reliability of the evaluations of the stability of the slope on the basis of the calculated safety factors (Fs). Three GPS points (P09, P15, P19) were selected (Fig. 2). These three points were selected because they were the nearest points to Section A-A'. Fig. 16 shows the variation of the surface displacements during the monitoring period. The X direction is the tendency of the slope, and the Y direction is the trend of the slope. Fig. 16 shows that, during the monitoring period, it was found that the surface displacements of all three points were small (< 10 mm). Fluctuations of the monitoring displacement were induced mainly by measuring error, and they were neglected. The displacement monitoring data indicated that the slope was steady during the monitoring period. Fig. 4 shows that the monitoring GL always was smaller than the critical GL, which was calculated by FEM during the monitoring period. The monitoring results of GL were consistent with the monitoring results of GPS, which indicated that the safety factors calculated by FEM were reliable.

4.3. Comparison of the proposed rainfall threshold with I-D thresholds and IDF curves

The empirical I-D thresholds were derived by plotting two characteristics of precipitation, intensity (mm/h or mm day^{-1}) and duration (h or day), that have or have not resulted in landslides in a given area. Then a separation line is drawn visually or by separation techniques to serve as a deterministic threshold or a probabilistic transition zone between precipitation events that induce landslides and events that do not involve such hazards. Due to the fact that the information is spread over several orders of magnitude, it usually is plotted on a bi-logarithmic scale. The IDF curves routinely are used in storm water and flood management design and predictions because they describe the relationship that links the duration and mean intensity of precipitation events characterized by the same return period (Bogaard and Greco, 2018). Several functional expressions can be used to describe such a relationship, most of which can be approximated, especially for durations longer than 1 h, as a power law:

$$I = A \times D^{B} \quad (6)$$

where I is the intensity of the rainfall (mm/h), D is the duration (h), B is the slope of the log-plotted straight line, and A is a measure of the rain intensity of a rain event of unit duration. Eq. (6) also is used to describe the precipitation ID thresholds, the difference being that the IDF curves

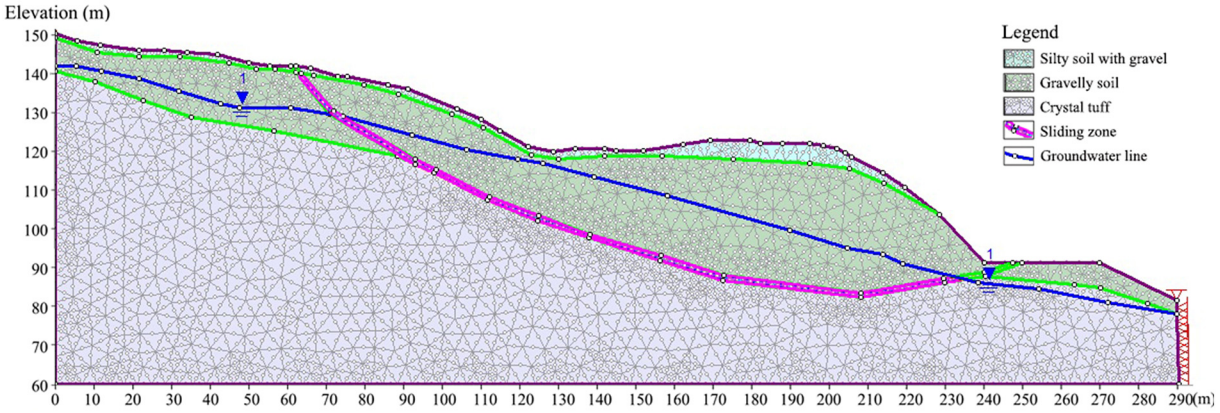

Fig. 15. Model of the initial stage of the numerical simulation.

Table 2
Properties of the soil and rock of the Duxiantou landslide (Sun and Lü, 2012).

Material	c (kPa)	φ (°)	γ (kN/m^3)	E (MPa)	μ
Silty soil with gravel	24	18.7	19.7	6.46	0.32
Gravelly soil	27	26.5	20.44	5.87	0.24
Sliding zone	14.5	12	19.7	1.5	0.35
Crystal tuff	294	38.9	24.43	22,000	0.2

NOTE: c is cohesion, φ is the fiction angle, γ is the unit weight, E is the modulus, and μ is Poisson's Ratio.

Table 3
Values of Fs for different values of GL of the Duxiantou landslide.

GL in ZK1 (m)	GL in ZK3 (m)	Fs
No groundwater	No groundwater	1.423
Investigation groundwater level (12.2)	Investigation groundwater level (18.2)	1.146
20.92	16.80	1.105
21.55	18.39	1.080
21.38	19.32	1.067
22.42	19.62	1.061
22.26	20.16	1.050
22.07	20.52	1.045

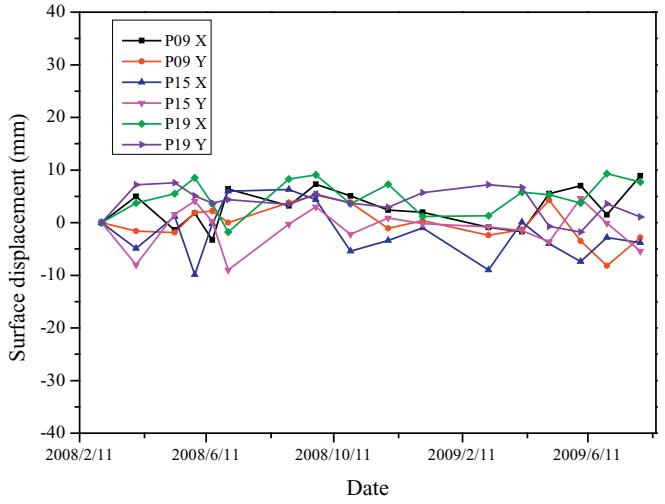

Fig. 16. Surface displacements of GPS points.

are isolines of the cumulative probability of precipitation events, whereas the ID plots are empirical thresholds for the occurrence of landslides and debris flows.

In this study, the IDF curves are determined based on the Atlas of Storms Statistical Parameters for Zhejiang Province (Zhejiang Province Bureau of Hydrology, 2003). The Atlas used the results of a Pearson type-III distribution to analyze the frequency of storms. The distribution of the IDF curves were determined based on the statistical results over many years from several meteorological stations. For different regions, the distribution of the IDF curves also was different. Note that the IDF curves and ID thresholds were determined, for the most part, for rain durations up to 24 h (Bogaard and Greco, 2018). So, in this study, the durations of the I-D threshold and the IDF curves were selected as1, 3, 6, and 24 h. Then, based on the Atlas, we could choose the specific IDF curves of the landslide site. In addition, in order to verify that the IDF curves that were used could reflect the actual rainfall characteristics of the landslide site, we compared the IDF curves that were used with the rainfall recorded at the Guantan station (Fig. 17). The five-year return period means the possible maximum precipitation in a five-year period. The three-year return period means the possible maximum precipitation in a three-year period. The duration of monitoring recording from Guantan station is approximately five years. So, if the maximum precipitation during monitoring recording is close to the precipitation of the five-year return period, it means the chosen IDF curves could reflect the actual rainfall characteristics at the landslide site. Fig. 17 indicates that the maximum precipitation of monitoring recording was larger than the three-year return period and slightly smaller than the five-year return period, except that the duration was 24 h. The actual maximum precipitation of monitoring recording at the Guantan station was close to the precipitation of the five-year return period from the IDF curves.

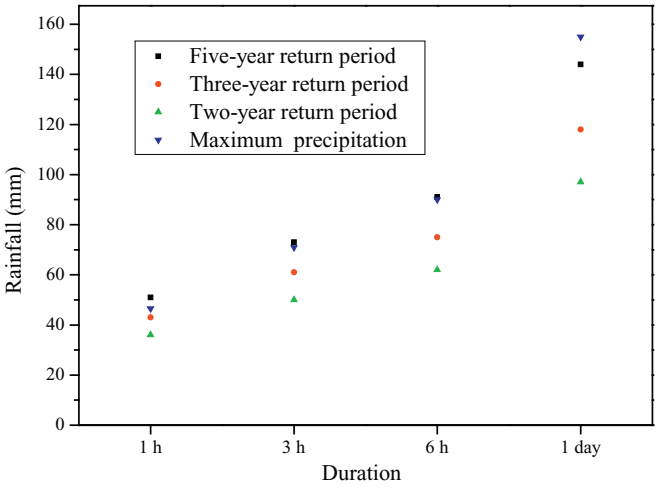

Fig. 17. Comparison of maximum precipitation with precipitation of different return periods.

Table 4
Values of Fs for different return period storms when the duration of the rainfall is 24 h.

Return period (year)	Peak GL in ZK1 (m)	Peak GL in ZK3 (m)	Fs
2	22.53	21.91	1.026
3	22.91	22.52	1.016
5	23.11	23.12	1.002
10	23.27	23.76	0.996
20	23.37	24.20	0.994
50	23.44	24.48	0.993
100	23.48	25.00	0.991

This means the chosen IDF curves could reflect the actual rainfall characteristics of the landslide site.

As we highlighted in 4.1.3, the antecedent rainfall can be important up to four days earlier. In order to consider the effect of antecedent rainfall, we used a precipitation process as the input parameter rather than only using precipitation data points. For different durations and different return periods, a precipitation process includes five precipitation time sequences. Each precipitation time sequence includes five precipitation data points (P0, P1, P2, P3, P4), with each precipitation data point representing the precipitation of one day. The four data points, i.e., P1, P2, P3, and P4 represent the antecedent rainfall before the event, and P0 represents the precipitation on that day. Then, we regarded the precipitation process as an input parameter for the GA-SVM model. We obtained five GL values for one precipitation process, and each calculated GL represents the results of its corresponding four days of antecedent rainfall. The largest GL will be the peak groundwater level in a precipitation process. Then, we selected the largest GL value as the input parameter of FE-SSR to explore the relationship between GL and Fs. The Fs also can be calculated using the FE-SSR method based on the computed variations of GL. Tables 4–7 provide the values of Fs computed for different return periods and different rainfall durations.

As shown in Table 4, when the rainfall duration is 24 h and the return period is five years, the Fs is 1.002, which means the slope is in a critical condition. When the return period is set to 10 years, the Fs is 0.996, which means the slope is unstable. Thus, the rainfall for the 10-year return period is the threshold of instability. When the duration is 6 h, the value of Fs is 0.998 since the return period is 50 years. When the value of Fs is < 1, the slope is in an unstable condition, so the rainfall for the 50-year return period is the threshold. When the durations are 3 h and 1 h, none of the rainfall events could cause the value of Fs to be < 1.

In order to verify the accuracy of the proposed model, we compared our results with the results of empirical I-D thresholds (Fig. 18). The ordinate of Fig. 18 is the average intensity of precipitation, and the abscissa is the duration of the rainfall. Ma et al. (2015) studied the impact of rainfall events of different durations on the occurrence of landslides based on 1569 landslides in Zhejiang Province from 1990 to 2013. They determined the rainfall intensity–duration (I-D) thresholds of 62 mountainous counties and cities in Zhejiang Province. The thresholds refer to a variety of types of landslides. For comparison, we chose the I-D threshold curve of Longyou City, which covers the study area used in this work, and the mean I-D threshold curve of Zhejiang Province, as shown in Fig. 18. The research of Ma et al. (2015) also provided the sole threshold in the study area.

Table 5
Values of Fs for different return period storms when the duration of the rainfall is 6 h.

Return period (year)	Peak GL in ZK1 (m)	Peak GL in ZK3 (m)	Fs
2	22.25	20.88	1.040
3	22.43	21.27	1.035
5	22.63	21.74	1.030
10	22.85	22.39	1.022
20	23.02	22.83	1.015
50	23.18	23.41	0.998
100	23.27	23.75	0.996

Table 6
Value of Fs for different return period storms when the duration of the rainfall is 3 h.

Return period (year)	Peak GL in ZK1 (m)	Peak GL in ZK3 (m)	Fs
2	22.09	20.54	1.042
3	22.23	20.83	1.038
5	22.40	21.20	1.034
10	22.60	21.65	1.028
20	22.76	22.09	1.023
50	22.95	22.61	1.014
100	23.06	22.95	1.009

Table 7
Value of Fs for different return period storms when the duration of the rainfall is 1 h.

Return period (year)	Peak GL in ZK1 (m)	Peak GL in ZK3 (m)	Fs
2	21.88	20.11	1.047
3	21.98	20.31	1.045
5	22.10	20.54	1.042
10	22.24	20.85	1.038
20	22.37	21.14	1.035
50	22.53	21.50	1.030
100	22.64	21.77	1.027

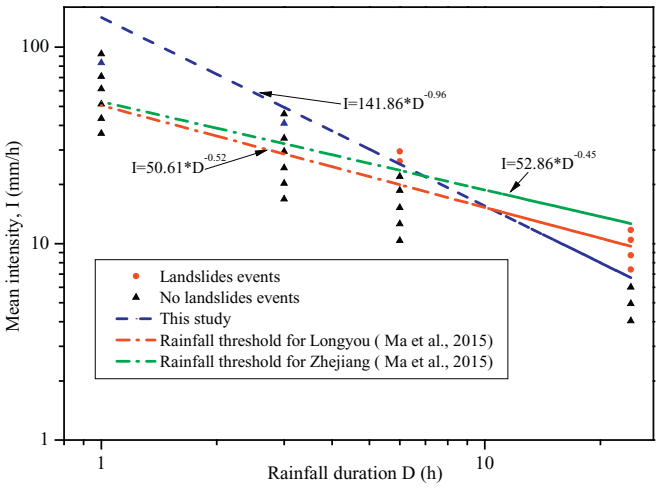

Fig. 18. Comparison of thresholds with those of another empirical study.

Fig. 18 shows that the thresholds proposed in this study are smaller than those in Ma et al. (2015) when the duration of the rainfall was relatively long, e.g., D = 24 h, which means the results of Ma et al. (2015) are risky for the Duxiantou landslides for long durations. For short durations, e.g., < 6 h, the proposed thresholds are larger than those of Ma et al. (2015). This means the results of Ma et al. (2015) are conservative for the Duxiantou landslides for short durations. We considered that this discrepancy might have been caused mainly by different landslide mechanisms. Most deep-seated landslides that are 5–20 m in depth are sensitive to rainfall and prone to sliding due to the increase in the pressure of the pore water on the slip surface induced by the rising groundwater level (Van Asch et al., 1999). The longer duration of the rainfall means the total amount of rainfall will be larger, resulting in larger increases in the groundwater level. So, when the duration is as long as 24 h, the rainfall threshold proposed in this study is smaller. The proposed model for deep-seated landslides is more sensitive for longer durations and larger amounts of rainfall. However,

for shallow landslides or debris flows, failure conditions also can occur when, at a critical depth that is determined mainly by the cohesion of the soil mass and the slope angle, the moisture content in the soil becomes close to saturation, resulting in a considerable reduction in the strength of the soil (Van Asch et al., 1999). Thus, the thresholds for triggering shallow landslides or debris flows usually are not sensitive to the total amount of rainfall; rather, there are controlled mainly by the intensity of the rainfall in a short period of time (Wei et al., 2017, 2018). This understanding also is in good agreement with that found in Dai and Lee (2001), who investigated magnitude–cumulative frequency relationship for landslides and the relationship between rainfall and the occurrence of landslides in Hong Kong. They concluded that, with an increase in the failure depth of landslides (from shallow landslides to deep-seated landslides), the most important rainfall variable may vary from short-duration rainfall (12-h rolling rainfall) to relatively long duration rainfall (24-h rolling rainfall). Ng et al. (2001) investigated groundwater responses in an initially unsaturated cut slope at Lai Ping Road in Hong Kong subjected to rainfalls with various patterns, durations, and return periods. The results showed that short-duration, intense rainfall causes larger variations in pore-water pressure at shallow depths, whereas long-duration rainfall has a greater influence on groundwater in deep soils because of the generally greater amount of rainfall. As we highlighted in Section 2, the Duxiantou landslide is a deep-seated landslide. Therefore, the proposed threshold is more suitable for deep-seated landslides than shallow landslides. However, in Ma's study, the statistical data contained both shallow and deep landslides, so the empirical model that was obtained is a more comprehensive model. That is the reason that the results of empirical model is smaller than the proposed model for short-duration rainfall and that its is larger than the proposed model for long-duration rainfall. Bogaard and Greco (2018) also considered that the current I-D concept mainly incorporates an unacceptably wide range of information with different types of hazards (debris flows and landslides related to different hydrological processes) and different temporal meteorological information (from minutes to several days). This makes the use of ID thresholds cumbersome or even misleading. Compared with these conventional empirical models, the proposed model improved the accuracy and reliability of the estimates of the thresholds of deep-seated landslides, which provides a novel approach for establishing warning systems for such landslides.

5. Conclusion

In this study, an integrated model was proposed to estimate the rainfall threshold by coupling the groundwater level predicting models with the finite element strength reduction model. First, we proposed a new method to calculate the value of the groundwater level fluctuation by rainfall (GLFR). Then, based on the continuous monitoring data of groundwater level (GL) and precipitation, two different machine learning methods, i.e., GA-BPNN and GA-SVM, were developed for the prediction of the GLFR of Duxiantou landslides in Zhejiang Province, China. The calculated results showed that the GA-SVM model performed better than the GA-BPNN model, so the GA-SVM model can be used to determine the relationship between preceding rainfall and GLFR. We also evaluated the effect of GLFD on forecasting the value of GLF. The results showed that there would be a negative effect on the calculation of GLF if the calculation of GLFD were ignored. The GA-SVM model indicated that RMSE increased from 0.089 to 0.144 and that RI decreased from 0.95 to 0.71. Then, based on the data acquired by monitoring groundwater level (GL), the FE-SSR model was used to investigate the factor of safety (Fs) of the slope at different groundwater levels. The results showed the GL has a significant effect on Fs. As the GL increased by 1 m, the value of Fs decreased by an average of 0.2. The probability of the occurrence of the Duxiantou Landslide with different return periods also was evaluated to determine the rainfall threshold.

Acknowledgments

This study was supported financially by the National Natural Science Foundation of China (Grant No. 41772276) and Key Research and Development Project of Zhejiang Province (Grant No. 2017C03006).

We gratefully acknowledge that Ms. Jinyao Yang helped us to improve the quality of pictures in this paper.

References

Baird, K.J., Iii, T.M., 2005. Simulating riparian evapotranspiration: a new methodology and application for groundwater models. J. Hydrol. 312 (1), 176–190.
Berti, M., Martina, M.L.V., Franceschini, S., Pignone, S., Simoni, A., Pizziolo, M., 2012. Probabilistic rainfall thresholds for landslide occurrence using a Bayesian approach. J. Geophy. Res. Earth Surf 117, F04006.
Bogaard, T., Greco, R., 2018. Invited perspectives: hydrological perspectives on precipitation intensity-duration thresholds for landslide initiation: proposing hydro-meteorological thresholds. Nat. Hazards Earth Syst. Sci 18 (1), 31–39.
Cai, Z., Xu, W., Meng, Y., Shi, C., Wang, R., 2016. Prediction of landslide displacement based on GA-LSSVM with multiple factors. Bull. Eng. Geol. Environ. 75 (2), 637–646.
Caris, J.P.T., Asch, T.W.J.V., 1991. Geophysical, geotechnical and hydrological investigations of a small landslide in the French Alps. Eng. Geol. 31 (3–4), 249–276.
Cascini, L., Calvello, M., Grimaldi, G.M., 2010. Groundwater modeling for the analysis of active slow-moving landslides. J. Geotech. Geoenviron. 136 (9), 1220–1230.
Cascini, L., Gullà, G., Sorbino, G., 2006. Groundwater modelling of a weathered gneissic cover. Can. Geotech. J. 43 (43), 1153–1166.
Cascini, L., Sorbino, G., Cuomo, S., Ferlisi, S., 2014. Seasonal effects of rainfall on the shallow pyroclastic deposits of the Campania region (Southern Italy). Landslides 11 (5), 779–792.
Chang, S.K., Lee, D.H., Wu, J.H., Juang, C.H., 2011. Rainfall-based criteria for assessing slump rate of mountainous highway slopes: a case study of slopes along highway 18 in Alishan, Taiwan. Eng. Geol. 118 (3–4), 63–74.
Cortes, C., Vapnik, V., 1995. Support-Vector Networks. Mach. Learn. 20 (3), 273–297.
Crosta, G., Prisco, C.D., 1999. On slope instability induced by seepage erosion. Can. Geotech. J. 36 (6), 1056–1073.
Dai, F.C., Lee, C.F., 2001. Frequency–volume relation and prediction of rainfall-induced landslides. Eng. Geol. 59 (3–4), 253–266.
Dawson, E.M., Roth, W.H., Drescher, A., 1999. Slope stability analysis by strength reduction. Géotechnique 49 (6), 835–840.
Federico, A., Elia, G., Fidelibus, C., Internò, G., Murianni, A., 2012. Prediction of time to slope failure: a general framework. Environ. Earth Sci 66 (1), 245–256.
Godt, J.W., Baum, R.L., Lu, N., 2009. Landsliding in partially saturated materials. Geophys. Res. Lett. 36 (2), 206–218.
Guzzetti, F., Peruccacci, S., Rossi, M., Stark, C., 2008. The rainfall intensity–duration control of shallow landslides and debris flows: an update. Landslides 5 (1), 3–17.
Han, Y., Zheng, F.L., Xu, X.M., 2017. Effects of rainfall regime and its character indices on soil loss at loessial hillslope with ephemeral gully. J. Mt. Sci. 14 (3), 527–538.
Hong, Y.M., 2017. Feasibility of using artificial neural networks to forecast groundwater levels in real time. Landslides (3–4), 1–12.
Hong, Y., Hiura, H., Shino, K., Sassa, K., Fukuoka, H., 2005. Quantitative assessment on the influence of heavy rainfall on the crystalline schist landslide by monitoring system -case study on Zentoku landslide, Japan. Landslides 2 (1), 31–41.
Hong, M., Kim, J., Jeong, S., 2017. Rainfall intensity-duration thresholds for landslide prediction in South Korea by considering the effects of antecedent rainfall. Landslides (5), 1–12.
Hong, Y.M., Wan, S., 2011. Forecasting groundwater level fluctuations for rainfall-induced landslide. Nat. Hazards 57 (2), 167–184.
Huang, F., Huang, J., Jiang, S., Zhou, C., 2017. Groundwater levels prediction using evidence of chaos and support vector machine. J. Hydroinf. 19 (4), jh2017102.
Iverson, R.M., 2000. Landslide triggering by rain infiltration. Water Resour. Res. 36 (7), 1897–1910.
Jan, C.D., Chen, T.H., Lo, W.C., 2007. Effect of rainfall intensity and distribution on groundwater level fluctuations. J. Hydrol. 332 (3), 348–360.
Ji, J., Zhang, C., Gui, Y., Lü, Q., Kodikara, J., 2016. New observations on the application of ls-svm in slope system reliability analysis. J. Comput. Civ. Eng. 31 (2) (06016002).
Krkač, M., Špoljarić, D., Bernat, S., Arbanas, S.M., 2017. Method for prediction of landslide movements based on random forests. Landslides 14 (3), 947–960.
Lee, D.H., Lai, M.H., Wu, J.H., Chi, Y.Y., Ko, W.T., Lee, B.L., 2013. Slope management criteria for Alishan highway based on database of heavy rainfall-induced slope failures. Eng. Geol. 162, 97–107.
Li, X.Z., Kong, J.M., 2014. Application of GA-SVM method with parameter optimization for landslide development prediction. Nat. Hazards Earth Syst. Sci. 14 (3), 5295–5322.
Lin, H.M., Chang, S.K., Wu, J.H., Juang, C.H., 2009. Neural network-based model for assessing failure potential of highway slopes in the Alishan, Taiwan area: pre- and post-earthquake investigation. Eng. Geol. 104 (3–4), 280–289.
Lin, H.M., Wu, J.H., Sunarya, E., 2018. Consolidated and undrained ring shear tests on the sliding surface of the Hsien-du-shan landslide in Taiwan. Geofluids 2018 (Article ID 9410890, 12 pages).
Lü, Q., Chan, C.L., Low, B.K., 2012. Probabilistic evaluation of ground-support interaction for deep rock excavation using artificial neural network and uniform design. Tunn.

Undergr. Space Technol. 32, 1–18.
Ma, T.H., Li, C.J., Lu, Z.M., Bao, Q.Y., 2015. Rainfall intensity–duration thresholds for the initiation of landslides in Zhejiang Province, Southeast China. Geomorphology 245, 193–206.
Mansour, M.F., Morgenstern, N.R., Martin, C.D., 2011. Expected damage from displacement of slow-moving slides. Landslides 8 (1), 117–131.
Mantovani, F., Pasuto, A., Silvano, S., Zannoni, A., 2000. Collecting data to define future hazard scenarios of the Tessina landslide. Int. J. Appl. Earth Obs. Geoinf. 2 (1), 33–40.
Marjanović, M., Kovačević, M., Bajat, B., Voženílek, V., 2011. Landslide susceptibility assessment using SVM machine learning algorithm. Eng. Geol. 123 (3), 225–234.
Martinović, K., Gavin, K., Reale, C., Mangan, C., 2018. Rainfall thresholds as a landslide indicator for engineered slopes on the Irish Rail network. Geomorphology 306, 40–50.
Matsuura, S., Asano, S., Okamoto, T., 2008. Relationship between rain and/or meltwater, pore-water pressure and displacement of a reactivated landslide. Eng. Geol. 101 (1), 49–59.
Ng, C.W., Wang, B., Tung, Y.K., 2001. Three-dimensional numerical investigations of groundwater responses in an unsaturated slope subjected to various rainfall patterns. Can. Geotech. J. 38 (5), 1049–1062.
Okada, Y., Sassa, K., Fukuoka, H., 2004. Excess pore pressure and grain crushing of sands by means of undrained and naturally drained ring-shear tests. Eng. Geol. 75 (3), 325–343.
Peruccacci, S., Brunetti, M.T., Gariano, S.L., Melillo, M., Rossi, M., Guzzetti, F., 2017. Rainfall thresholds for possible landslide occurrence in Italy. Geomorphology 290, 39–57.
Pirone, M., Papa, R., Nicotera, M.V., Urciuoli, G., 2015a. In situ monitoring of the groundwater field in an unsaturated pyroclastic slope for slope stability evaluation. Landslides 12 (2), 259–276.
Pirone, M., Papa, R., Nicotera, M.V., Urciuoli, G., 2015b. Soil water balance in an unsaturated pyroclastic slope for evaluation of soil hydraulic behaviour and boundary conditions. J. Hydrol. 528, 63–83.
Schilling, K.E., 2009. Investigating local variation in groundwater recharge along a topographic gradient, Walnut Creek, Iowa, USA. Hydrogeol. J. 17 (2), 397–407.
Simoni, A., Berti, M., Generali, M., Elmi, C., Ghirotti, M., 2004. Preliminary result from pore pressure monitoring on an unstable clay slope. Eng. Geol. 73 (1), 117–128.
Sun, H.Y., Lü, Q., 2012. Formation Mechanism and Prevention of Colluvial Landslide. Science Press, pp. 157–176 (in Chinese).
Sun, H.Y., Wong, L.N.Y., Shang, Y.Q., Yu, B.T., Wang, Z.L., 2012. Experimental studies of groundwater pipe flow network characteristics in gravelly soil slopes. Landslides 9 (4), 475–483.
Urciuoli, G., Pirone, M., Comegna, L., Picarelli, L., 2016. Long-term investigations on the pore pressure regime in saturated and unsaturated sloping soils. Eng. Geol. 212, 98–119.
Van Asch, T.W.J., Buma, J., Beek, L.P.H.V., 1999. A view on some hydrological triggering systems in landslides. Geomorphology 30 (1–2), 25–32.
Wei, Z.L., Shang, Y.Q., Zhao, Y., Pan, P., Jiang, Y.J., 2017. Rainfall threshold for initiation of channelized debris flows in a small catchment based on in-site measurement. Eng. Geol. 217, 23–34.
Wei, Z.L., Xu, Y.P., Sun, H.Y., Xie, W., Wu, G., 2018. Predicting the occurrence of channelized debris flow by an integrated cascading model: a case study of a small debris flow-prone catchment in Zhejiang province, China. Geomorphology 308, 78–90.
Yoon, H., Jun, S., Hyun, Y., Bae, G., Lee, K., 2011. A comparative study of artificial neural networks and support vector machines for predicting groundwater levels in a coastal aquifer. J. Hydrol. 396 (1), 128–138.
Zhang, L.L., Fredlund, M., Fredlund, D.G., Lu, H.H., Wilson, G.W., 2015. The influence of the unsaturated soil zone on 2-D and 3-D slope stability analyses. Eng. Geol. 193, 374–383.
Zhang, J., Wang, H., Huang, H.W., Chen, L.H., 2017. System reliability analysis of soil slopes stabilized with piles. Eng. Geol. 229, 45–52.
Zhejiang Province Bureau of Hydrology, 2003. Atlas of Storms Statistical Parameters for Zhejiang Province. Hangzhou, Zhejiang. (in Chinese).
Zhi, M.M., Shang, Y.Q., Zhao, Y., Lü, Q., Sun, H., 2016. Investigation and monitoring on a rainfall-induced deep-seated landslide. Arab. J. Geosci. 9 (3), 182.
Zhou, C., Yin, K., Cao, Y., Ahmed, B., 2016. Application of time series analysis and PSO–SVM model in predicting the Bazimen landslide in the three Gorges Reservoir, China. Eng. Geol. 204, 108–120.